The Impact of Influenza Hemagglutinin Fusion Peptide Length and Viral Subtype on Its Structure and Dynamics

Justin L. Lorieau, John M. Louis, Ad Bax
Laboratory of Chemical Physics, National Institute of Diabetes and Digestive and Kidney Diseases, National Institutes of Health, Bethesda, MD 20892

Received 30 April 2012; accepted 25 May 2012
Published online 7 June 2012 in Wiley Online Library (wileyonlinelibrary.com). DOI 10.1002/bip.22102

ABSTRACT:

A peptide comprising no fewer than the first 20 residues of the influenza hemagglutinin HA2 subunit suffices to induce lipid mixing between the membranes of different unilamellar vesicles. This 20-residue peptide was previously reported to adopt an open "boomerang" structure that differs significantly from the closed helical-hairpin structure of a fusion peptide consisting of the first 23 residues of the HA2 sequence. This study investigates the structural and dynamic features of fusion peptides of different length and subtype. Lacking key interactions that stabilize the closed, helical-hairpin structure, the 20-residue peptide is in a dynamic equilibrium between closed and open states, adopting a ca. 11% population of the former when solubilized by DPC micelles. Peptides shorter than 20 residues would have even fewer interactions to stabilize a helical hairpin fold, resulting in a vanishing hairpin population. Considering the conserved nature of hairpin-stabilizing interactions across all serotypes, and the minimum of 20 residues needed for fusion, we postulate that the closed state plays an essential role in the fusion process. However, opening of this hairpin structure may be essential to the formation of a membrane pore at the final stage of the fusion process. Published 2012 Wiley Periodicals, Inc. Biopolymers 99: 189–195, 2013.*

Keywords: *NMR; chemical shift; dynamics; boomerang; hairpin*

This article was originally published online as an accepted preprint. The "Published Online" date corresponds to the preprint version. You can request a copy of the preprint by emailing the Biopolymers editorial office at biopolymers@wiley.com

INTRODUCTION

The influenza hemagglutinin glycoprotein is embedded in the viral membrane and has a homotrimeric structure, with each monomer consisting of two subunits, HA1 and HA2, which are responsible for fusing the viral membrane with the host-cell endosomal membrane during the infection process.[1,2] A drop in pH in the endosome produces a large, "spring-loaded" conformational change in the hemagglutinin that extrudes a highly hydrophobic and highly conserved sequence on the N-terminus of the coiled-coil trimer of HA2.[3,4] This sequence, known as the hemagglutinin fusion peptide, anchors into the endosomal membrane to initiate the fusiogenic process.[5] Even conservative truncations or mutations in this sequence have been shown to completely abrogate fusion activity.[6,7]

It has long been known that a fusion peptide consisting of the first 20 residues of the H3 subtype of HA2, H3-HAfp20, can promote lipid mixing of large unilamellar-vesicles (LUVs)[8] and cause rapid and efficient fusion of phosphatidylcholine vesicles.[9] Extensive studies were conducted on the fusion activity[9,10] structure,[11–15] membrane integration[12,16–19] and simulation behavior[20–22] of this

Additional Supporting Information may be found in the online version of this article.

Correspondence to: Dr. Ad Bax; e-mail: bax@nih.gov

Contract grant sponsors: Intramural Research Program of the National Institute of Diabetes and Digestive and Kidney Diseases, National Institutes of Health (NIH), and the Intramural AIDS-Targeted Antiviral Program of the Office of the Director, NIH

peptide to better understand its role in promoting membrane fusion.

However, comparison of the amino acid sequence of 16 hemagglutinin subtypes shows that the conserved region of the fusion peptide sequence extends to at least 25 residues.[23] Indeed, it was found that a fusion peptide comprising the first 23 residues of the swine flu variant (H1-subtype), H1-HAfp23, adopts a helical-hairpin structure,[24] which differs significantly from the open "boomerang" structure reported for H3-HAfp20.[25]

Despite the large differences in the structures of H3-HAfp20 and H1-HAfp23, both peptides are fusiogenic as evaluated by lipid mixing assays.[26] However, the question remains: what is common between these two peptides, and how can they both catalyze membrane fusion? A closely related question "why are these two structures different?" also remains unanswered.

In this study, we aim to address these questions by studying the chemical, structural and dynamical properties of hemagglutinin fusion peptides of different length and subtype. We report on the similarities and differences between the H1- and H3-subtypes of HAfp20, and explore the structural consequences of shortening and extending the length of the fusion peptide. We find that the structure of H1-HAfp20 is highly dynamic and rapidly switches between a minor population that adopts a 'closed', hairpin-like conformation of H1-HAfp23, but mostly exists in an "open" conformation where its two helices remain flexibly tethered, with significant fraying of the second helix towards its C-terminal end.

MATERIALS AND METHODS

NMR Sample Preparation

Fusion peptides were expressed in *Escherichia coli* as fusion proteins linked to the IgG-binding domain B1 of streptococcal protein G (GB1), which included an N-terminal His-tag and a C-terminal factor Xa protease cleavage site flanking GB1. Details regarding the expression, purification and isotopic labeling have been described previously.[24] The various fusion peptides studied had the following sequences:

H3-HAfp20: GLFGAIAGFIENGWEGMIDGSGKKKKD
H1-HAfp14: GLFGAIAGFIEGGWKKKKD
H1-HAfp20: GLFGAIAGFIEGGWTGMIDGSGKKKKD
H1-HAfp23: GLFGAIAGFIEGGWTGMIDGWYGSGKKKKD
H1-HAfp28: GLFGAIAGFIEGGWTGMIDGWYGYHHQNSGKKKKD

The underlined sequences constitute the highly charged "host" component of the so-called host-guest system, introduced to facilitate sample preparation and study of the highly hydrophobic fusion peptides.[27] Samples for NMR were expressed with [^{15}N]-, [^{13}C,^{15}N]- and [^{2}H,^{13}C,^{15}N]- isotopic labeling schemes and prepared to final concentrations of 0.3–0.6 m*M* peptide in 130–150 m*M* perdeuterated dodecylphosphocholine (DPC, Anatrace), 93% H_2O/7% D_2O, or 99.9% D_2O (for measurement of 2D NOESY spectra) and 25 mM ^{2}H-Tris at pH 7.3 ± 0.1 (Cambridge Isotopes), and a final volume of 280 μL in Shigemi microcells.

NMR Data Collection and Analysis

All experiments were conducted at 32°C on Bruker 600 MHz, 800 MHz or 900 MHz spectrometers, each equipped with a cryogenically cooled probe and a self-shielded z-gradient accessory. Chemical shift assignments were determined using gradient-enhanced ^{15}N-HSQC, HNCA, HNCO, and constant-time ^{13}C-HSQC experiments, as well as a ^{1}H-^{1}H 2D NOESY experiment. The ^{1}H-^{1}H 2D NOESY experiments (T_{mix} = 70 ms) were carried out at 900 MHz on ^{15}N-labeled peptides in 99.9% $^{2}H_2O$, using a 10 Hz presaturating radio-frequency field on the HDO resonance between transients. Chemical shift assignments are included as Supporting Information.

The ^{15}N R_1, R_2, and ^{15}N-{^{1}H} NOE relaxation measurements were measured at 600 MHz using a gradient-enhanced ^{15}N-HSQC sequence.[28] Analysis of relaxation rates was conducted using the program Model-Free,[29] assuming an axially symmetric ^{15}N CSA of -173 ppm,[30] a ^{1}H-^{15}N libration-corrected bond length of 1.04 Å,[31] and an isotropic diffusion model. A minimum threshold error of 3.5% was used for all relaxation data.

RESULTS AND DISCUSSION

Comparison of the H1- and H3-Serotype Peptides

The H3-HAfp20 fusion peptide differs from the H1-HAfp20 sequence by two mutations, N12G and E15T. Except for these two mutated residues, the backbone ^{15}N-^{1}H HSQC spectra (Figure 1) reveal closely similar chemical shifts for the two peptides, indicative of a very high degree of similarity in their structures. As expected, substantial chemical shift changes occur at the sites of mutation, residues 12 and 15, reflecting the impact of the difference in covalent structure on chemical shift, as well as small differences for the immediately adjacent residues.

The detailed biophysical characterization of the H3 fusion peptide by lengthy NMR experiments is complicated by the limited stability of this peptide. Unless special precautions are taken, partial chemical modification resulting from a deamidation reaction at Asn-12 takes place during peptide purification, and continues once the purified peptide is in the NMR sample tube, solubilized by (DPC) micelles. Intramolecular deamidation of Asn, is accelerated when followed by a Gly residue and results in multiple end-products, including conversion through a succinimide intermediate to L-Asp, D-Asp, and iso-Asp.[32] The degradation products for the H3-HAfp20 sample give rise to numerous additional small peaks in the HSQC NMR spectrum and can clearly be seen in Figure 1, and the presence of deamidation was confirmed by

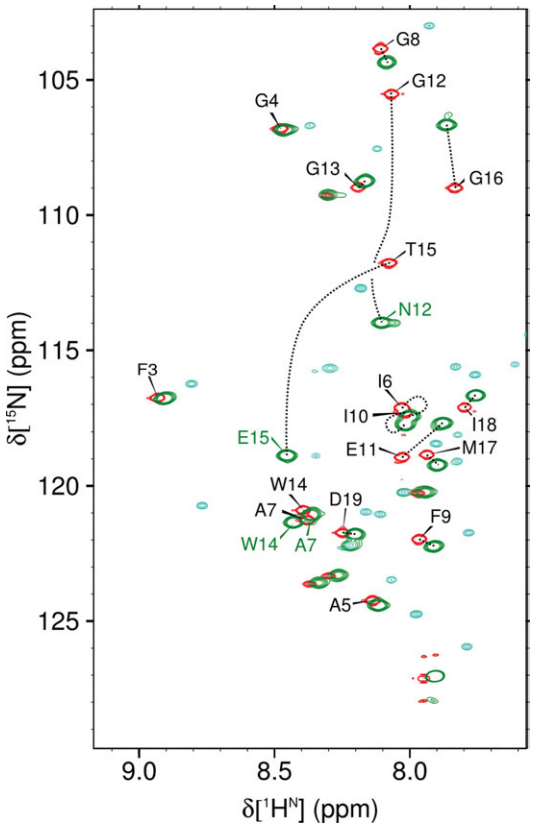

FIGURE 1 Superimposed ^{1}H-^{15}N HSQC spectra of the H1-subtype (red) and H3-subtype (green) for the HAfp20 peptide. Assignments for the H1-subtype are marked in black, with dotted lines connecting the corresponding resonance for the H3-subtype. Minor cyan-colored peaks in the H3-subtype spectrum have no counterpart in the H1-subtype spectrum and correspond to degraded peptide, mostly deamidated at residue N12. Spectra were collected at pH 7.3 ± 0.1, 600 MHz, 32°C.

Edman degradation peptide sequencing. The H1-subtype, which contains a Gly instead of an Asn residue in position 12, was therefore used for further study.

Chemical Shift Comparisons Between HAfp14, HAfp20, HAfp23, and HAfp28

The ^{15}N-HSQC spectra of four peptides of varying length, HAfp14, HAfp20, HAfp23 and HAfp28 (where the number of residues starting from the N-terminus of the HA2 domain of hemagglutinin is included in the name), all of the H1-subtype, are presented in Figure 2. The shorter peptides, HAfp14 and HAfp20, and the longer peptides, HAfp23 and HAfp28, have chemical shifts that closely group together, implying that the two shorter peptides are structurally similar to one another, as are the two longer ones, but that these two types of structures are distinctly different from one another. Indeed, this observation is consistent with a helical-hairpin structure found for HAfp23,[33] versus a more open two-helix structure reported for HAfp20.[25]

The differences between the shorter and longer constructs are also evident in their fast-timescale dynamic behaviors. Figure 3 presents the backbone ^{15}N relaxation data for HAfp20, HAfp23 and HAfp28. The ^{15}N relaxation rates are sensitive to N—H bond vector motions on the ps-ns timescale. Using conventional Lipari-Szabo model-free analysis[34] of these rates, the overall elevated R_1 and decreased R_2 values for HAfp20 yields a shorter overall rotational correlation time (7.1 ± 0.1 ns) than is obtained with the same analysis for HAfp23 (8.4 ± 0.1 ns) and HAfp28 (8.4 ± 0.1 ns). This difference is somewhat larger than expected on the basis of the different sizes of the micelle-peptide aggregates, and instead may be attributed to motion of the peptide relative to the micelle. By increasing the size of the micelle to a bicelle, consisting of mixed lipids and detergent, we previously found for HAfp23 that the helical hairpin structure actually undergoes rigid body motions of considerable amplitude relative to the phospholipid aggregates, on a time scale of ca. 5 ns.[26] Such motions are not easily detected without measuring the relaxation rates as a function of size, and if not recognized mask themselves as a shortening of the overall rotational correlation time. It is therefore possible that the shorter apparent correlation time of 7.1 ns also is a result of such motions of the peptide relative to the micelle. Considering that HAfp20 adopts a more flexible, open structure, in which the two helices can move relative to one another, it is indeed likely that the angular excursions of its two helices relative to the micelle are larger than for the rigid hairpin structure, and they may also be somewhat more rapid.

When ^{15}N relaxation data are evaluated by the classic Lipari-Szabo model-free approach,[34] the resulting generalized backbone order parameters, S^2, which are a measure of rapid, sub-ns internal fluctuations of the ^{15}N-^{1}H bond vector orientations, can range from $S^2 = 1.0$, i.e. static, perfect order, to $S^2 = 0.0$ for complete isotropic disorder.[34] S^2 values extracted from the ^{15}N relaxation rates collected for HAfp20 and HAfp23, show that residues 3–12 of both peptides are relatively static. Secondary ^{13}C chemical shifts observed for these residues are fully compatible with the α-helical backbone conformations observed in the structures of H3-HAfp20[25] and HAfp23.[24] For HAfp23, the high degree of order is also seen for residues 14–23, but for HAfp20 the backbone amide groups in the second helix are exhibiting increasing amplitudes of internal motion when approaching the C-terminus (Figure 3). As shown in the bottom panel of Figure 3, the decrease in ^{15}N order parameters derived from relaxation data for HAfp20, closely matches the apparent order parameter, RCI-S^2, derived from backbone chemical

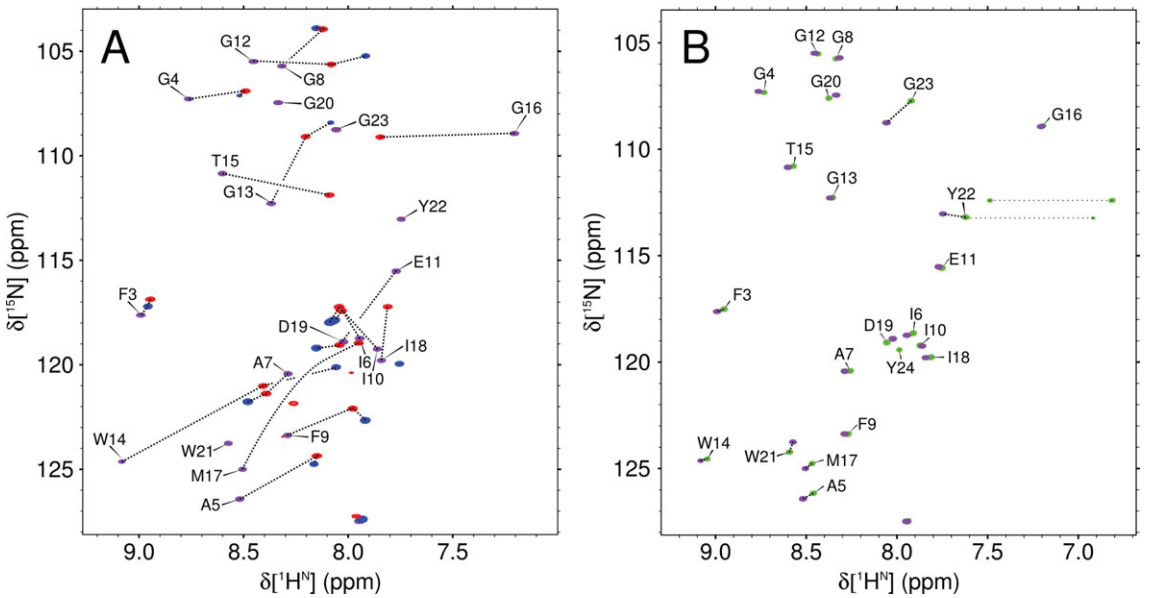

FIGURE 2 ^{1}H -^{15}N HSQC spectra of HAfp14 (blue), HAfp20 (red), HAfp23 (purple) and HAfp28 (green), recorded at pH 7.3 ± 0.1, 600 MHz, 32°C. A: Superposition of HAfp14, HAfp20, and HAfp23. Dotted lines have been used to link corresponding peaks, with assignments indicated for HAfp23. Amide signals of several of the host peptide residues of HAfp14 and the overlapped C-terminal residues of the host tags (at 7.95/127 ppm) have not been marked with assignments. B: Superimposed spectra of HAfp23 and HAfp28. Dotted lines have been used to link peaks of the corresponding pairs of residues and show that significant chemical shift changes are limited to the C-terminal residues Y22 and G23. Thin horizontal dotted lines link the geminal sidechain NH_2 resonances (yellow) of Q27 and of N28. Residues 25–28 of HAfp28 and of the host peptide sequence are dynamically disordered and not visible at pH 7.3 due to fast exchange with water.

shifts using a protocol described by Wishart and Berjanskii,[35] and implemented in the program TALOS+.[36] This observation is potentially interesting considering that the chemical shift derived order parameters reflect only those motions that impact chemical shifts, regardless of the rate at which they take place, and are insensitive to rigid body motions. By contrast, the ^{15}N relaxation derived values correspond to motions on a sub-ns time scale. The close correspondence of the order parameters derived from chemical shifts and from relaxation therefore indicates that the decrease in S^2 observed towards the C-terminus is dominated by sub-ns internal motion and not by rigid body motion of an intact helical fragment.

Residual Helical-Hairpin Structure in HAfp20

The helical hairpin structure of HAfp23 is stabilized by four aliphatic $C^{\alpha}H^{\alpha}$—O hydrogen bonds,[24] as well as a charge-dipole interaction between the N-terminal amino group and the dipole moment of the second helix, and potential direct H-bond interactions to its C-terminal carbonyl groups.[33]

In the HAfp20 construct, truncation of the last turn of the second helix sacrifices one $C^{\alpha}H^{\alpha}$—O interhelical hydrogen bond, from G1 to W21, as well as the interactions involving the G1 α-amino group. Three aliphatic hydrogen bonds could potentially remain if the structure were to stay otherwise intact, including two between A5 and M17 and one between F9 and G13. These remaining tertiary interactions apparently are insufficiently strong to lock HAfp20 into a permanently closed, hairpin-like structure. However, evidence of a minor population of the hairpin form can be found by inspecting the NOE spectrum at low contour levels. Figure 4 compares a few of the characteristic long-range NOE interactions, observed in 900 MHz 2D ^{1}H-^{1}H NOESY spectra of HAfp23 and HAfp20.

For HAfp23, the close proximity of its two helices is clearly illustrated by the intense interhelical NOEs between A5-H^{β}/M17-H^{α} and A5-H^{β}/W21-H^{α}, which are within 4 Å and 3 Å, respectively, of each other. The A5-H^{β}/W21-H^{α} NOE has 48% the intensity of the intraresidue A5-H^{β}/A5-H^{α} NOE. These long-range NOEs can still be observed in the HAfp20 construct, albeit at much lower intensity. The A5-H^{β}/S21-H^{α} NOE (where S21 is actually part of the "host"

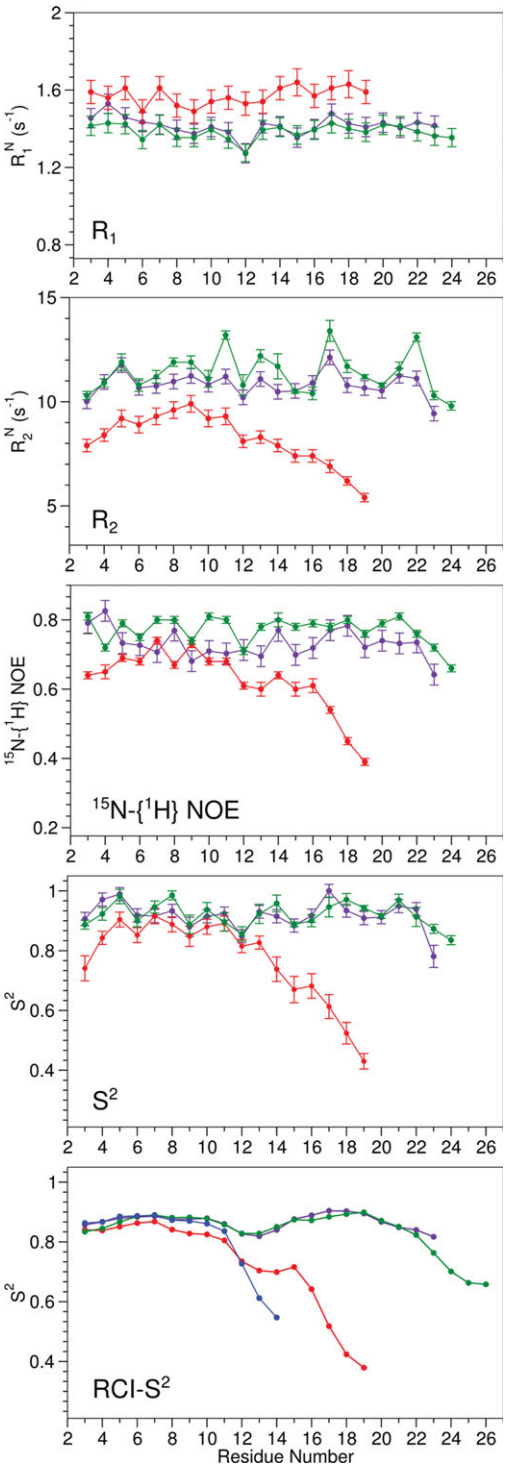

FIGURE 3 Backbone ^{15}N R_1, R_2 and ^{15}N-{^1H} NOE rates for HAfp20 (red), HAfp23 (purple) and HAfp28 (green) peptides. Relaxation rates were measured at 32°C and pH 7.4 ± 0.1 at 600 MHz. Relaxation rates were fitted using Lipari-Szabo[34] spectral density expressions and the Model-Free software package,[29] yielding the generalized order parameters S^2. For comparison, the chemical shift derived RCI-S^2 values[35] are shown in the bottom panel with the same corresponding colors, including HAfp14 (blue).

peptide) has an intensity of 4% relative to the intraresidue A5-H$^{\beta}$/A5-H$^{\alpha}$ NOE, and the intraresidue A5-H$^{\beta}$/M17-H$^{\alpha}$ NOE has a 1.5% relative intensity. The ca. 10-fold attenuation in interhelical NOE intensity suggests the presence of a closed conformer population of ~10%, with interchange between closed and open states occurring on a timescale slower than the overall rotational correlation time of the peptide:DPC complex, but much faster than the differences in chemical shift frequencies (on the order of a kHz) between the open and closed conformers, such that single resonances are observed which reflect the time-averaged chemical shifts.

Provided conformational exchange between the open and closed forms of HAfp23 takes place on a sub-millisecond time scale or faster, the time-averaged $^1H^N$ and ^{15}N chemical shifts observed for HAfp20 are not impacted by the time scale on which these motions take place, whereas the spectral densities that impact the NOE strength can be impacted by these rates. In the limit of fast exchange, chemical shift values simply reflect the population-weighted average of the states sampled by the molecule, and therefore can be used to obtain an accurate estimate of the closed-state population for HAfp20. The fast exchange condition is indeed fulfilled, as the HAfp20 peptide gives rise to sharp resonances at chemical shifts that fall, on average, between the chemical shifts of HAfp23, the closed state, and a severely truncated peptide,

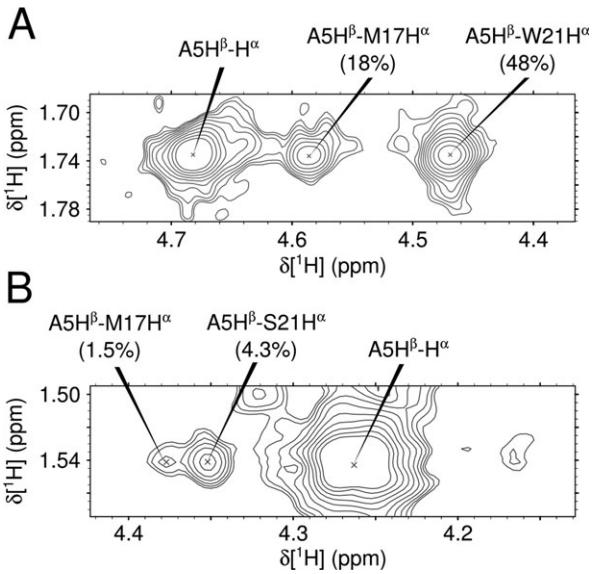

FIGURE 4 Expanded regions of the 2D 900 MHz NOESY spectra showing long-range interhelical contacts between residues 5, 17, and 21 for (A) HAfp23 and (B) HAfp20. Included under the resonance assignments are the intensities of the NOE cross peaks relative to the intraresidue A5-H$^{\beta}$/H$^{\alpha}$ peak. Spectra were recorded at pH 7.4 with an NOE mixing time of 70 ms. The region in (B) has a contour level cutoff 2.5 times lower than (A), relative to the A5-H$^{\beta}$/H$^{\alpha}$ cross peak.

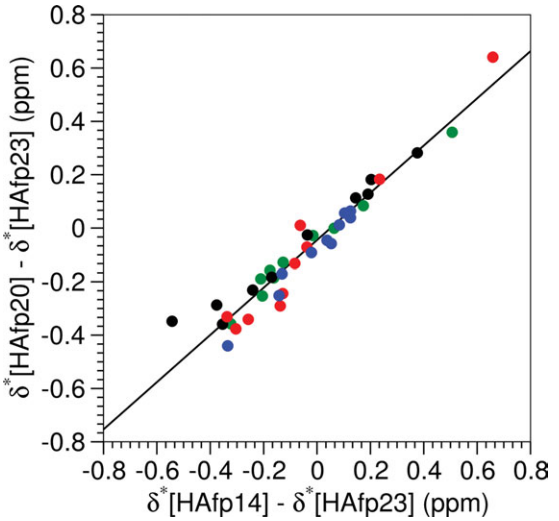

FIGURE 5 Correlation plot of the normalized chemical shift differences of HAfp20 and HAfp14 relative to HAfp23, using chemical shifts from residues 3 to 12. The approximately linear correlation indicates that HAfp20 chemical shifts correspond to a fast-limit, population-weighted average between open (HAfp14), and closed (HAfp23) states. The slope of the linear regression, fitted from equation 1, yields an open conformer population of 89 ± 4%. The chemical shifts of different nuclei types have been scaled by the following factors derived from protein database chemical shift distribution widths: $^{1}H^{N}$ = 1.0 (black), ^{15}N = 0.181 (red), $^{13}C^{\alpha}$ = 0.315 (blue), $^{13}C'$ = 0.376 (green).

HAfp14. The HAfp14 peptide remains α-helical through to residue 14, as judged by its secondary chemical shifts, but it lacks the second helix, and its remaining resonances therefore fully reflect an open state without interactions to a C-terminal helix. Plotting the HAfp20 chemical shifts together with the chemical shifts of the closed and open state, the population of the open state, p_{open}, can be determined from:

$$(\delta^*[\text{HAfp20}] - \delta^*[\text{closed}]) = p_{open}(\delta^*[\text{open}] - \delta^*[\text{closed}]), \quad (1)$$

where δ^* refers to the chemical shift of a given nucleus in either HAfp23 (closed), HAfp14 (open), or HAfp20. Because the range in chemical shifts, δ, varies for different types of nuclei, a scaled chemical shift, δ^*, was used by normalizing the chemical shift differences by factors of 1.00, 0.181, 0.376, and 0.315 for $^{1}H^{N}$, ^{15}N, $^{13}C'$, and $^{13}C\alpha$ nuclei, respectively, where these scaling factors are proportional to the inverse of the width of their distributions in the protein chemical shift database. A plot of Eq. (1) is presented in Figure 5.

As can be seen from this figure, the HAfp20 chemical shifts fall between the HAfp14 and HAfp23 chemical shifts with a best-fit open conformation population of 89 ± 4% and suggests that the HAfp20 exists as a conformational mixture of open and closed states that interchanges on a submillisecond timescale. Furthermore, the closed-conformation population of 11 ± 4% is in good agreement with the ca 10% population estimated above from the NOE measurements, though the NOE population values may be underestimated if the conformational exchange rate occurs on a time scale that impacts the J(0) spectral density. It is interesting to note that when using the classical NMR structure determination protocol,[14,15] where we attempt to find a single structure that is compatible with the NOE data (without consideration of the RDC data) an intermediate V-shaped or "boomerang-like" structure is obtained that is intermediate between the open and closed states. In such a single structure refinement, the angle between the two helices increases when the closed conformation is destabilized, as applies for the HAfp20 truncation mutation and other hairpin-destabilizing mutations, because the population-weighted NOEs from the closed structure become more attenuated. However, such "static structures" are incompatible with the RDC data, and also yield violations for the weak long-range NOE interactions between, for example, residues 5 and 21, which for predominantly open structures are only visible at very low contour levels.

CONCLUDING REMARKS

We have shown that residues 17–23 contribute key interactions that stabilize the helical-hairpin structure, observed for HAfp23. Without these residues, the closed conformation is destabilized and truncated peptides exist as a conformational mixture of closed and open states. For HAfp20, these conformations interchange on a timescale much faster than milliseconds. In addition, ^{15}N-NMR relaxation rates indicate that the decrease in secondary chemical shifts towards the C-terminal end of the second helix is associated with fraying of this second helix, with increasing amplitudes of the angular backbone motions on a timescale faster than the overall rotational correlation time of 7.1 ns.

The decrease in helical–hairpin population in the truncated peptides could explain the strict conservation of these residues and the importance of the helical–hairpin structure in the fusion mechanism. Although the HAfp20 peptide is fusiogenic, further truncations to the C-terminal helix eliminate lipid mixing fusion activity.[8] The nonfusiogenic HAfp16 is truncated by an additional four residues, thereby eliminating another two of the hairpin-stabilizing aliphatic $C^{\alpha}H^{\alpha}$—O hydrogen bonds, between A5 and M17. With HAfp14 being much too short for adopting a helical hairpin conformation, its lack of fusiogenic activity is therefore not surprising.

It also is conceivable, however, that the ability of the fusion peptide to exist in both an open and a closed states is key to its

function, and may relate to its dual role in first aiding in the generation of a hemi-fusion state, and subsequent opening to aid in generation of a pore in the endosomal membrane which connects the viral contents to the cytosol. The presence of such pores has been postulated to consist of a large cylinder, made up of helices that include both the fusion peptide of HA2 and its C-terminal transmembrane anchoring helix.[37,38] In such an arrangement, the fusion peptide would have to adopt an open state of sufficient length to traverse the membrane.[6]

Remarkably, despite the fact that HA2 residues 24–26 are highly conserved, adding these to the fusion peptide has no significant impact on its structure. The additional residues, incl. H25 and H26, have near random coil chemical shifts, and exhibit rapid backbone amide hydrogen exchange with solvent, indicative of the absence of stable hydrogen bonding. Together with negative ^{15}N-$\{^1H\}$ heteronuclear NOE values for H25 and H26, these data suggest random coil behavior for this region of the peptide. However, it is conceivable that in the native environment of the homotrimeric intact HA2 protein these residues become ordered, and that protonation of these residues upon acidification of the endosome contributes to a destabilization of the hairpin structure, and thereby to triggering the pore formation. However, considering that H26 is making stabilizing interactions in the prefusion hemagglutinin structure,[39] it is more likely that its conserved nature is related to expulsion of the fusion peptide in the prefusion to fusion transition of the protein.

The authors thank Annie Aniana for help with protein expression and purification, and Dennis Torchia and Attila Szabo for many helpful discussions, and acknowledge support from the NIDDK mass spectrometry facility.

REFERENCES

1. Wilson, I. A.; Skehel, J. J.; Wiley, D. C. Nature 1981, 289, 366–373.
2. Chernomordik, L. V.; Kozlov, M. M. Annu Rev Biochem 2003, 72, 175–207.
3. Carr, C. M.; Kim, P. S. Cell 1993, 73, 823–832.
4. Eckert, D. M.; Kim, P. S. Annu Rev Biochem 2001, 70, 777–810.
5. Kozlov, M. M.; Chernomordik, L. V. Biophys J 1998, 75, 1384–1396.
6. Armstrong, R. T.; Kushnir, A. S.; White, J. M. J Cell Biol 2000, 151, 425–437.
7. Cross, K. J.; Langley, W. A.; Russell, R. J.; Skehel, J. J.; Steinhauer, D. A. Protein Pept Lett 2009, 16, 766–778.
8. Lear, J. D.; Degrado, W. F. J Biol Chem 1987, 262, 6500–6505.
9. Murata, M.; Sugahara, Y.; Takahashi, S.; Ohnishi, S. J Biochem (Tokyo, Jpn) 1987, 102, 957–962.
10. Steinhauer, D. A.; Wharton, S. A.; Skehel, J. J.; Wiley, D. C. J Virol 1995, 69, 6643–6651.
11. Tamm, L. K.; Han, X.; Li, Y. L.; Lai, A. L. Biopolymers 2002, 66, 249–260.
12. Luneberg, J.; Martin, I.; Nussler, F.; Ruysschaert, J. M.; Herrmann, A. J Biol Chem 1995, 270, 27606–27614.
13. Zhou, Z.; Macosko, J. C.; Hughes, D. W.; Sayer, B. G.; Hawes, J.; Epand, R. M. Biophys J 2000, 78, 2418–2425.
14. Lai, A. L.; Park, H.; White, J. M.; Tamm, L. K. J Biol Chem 2006, 281, 5760–5770.
15. Lai, A. L.; Tamm, L. K. J Biol Chem 2007, 282, 23946–23956.
16. Macosko, J. C.; Kim, C. H.; Shin, Y. K. J Mol Biol 1997, 267, 1139–1148.
17. Epand, R. M.; Epand, R. F. Biochem Biophys Res Commun 1994, 202, 1420–1425.
18. Epand, R. M.; Epand, R. F. Biopolymers 2000, 55, 358–363.
19. Sun, Y.; Weliky, D. P. J Am Chem Soc 2009, 131, 13228–13229.
20. Lague, P.; Roux, B.; Pastor, R. W. J Mol Biol 2005, 354, 1129–1141.
21. Sammalkorpi, M.; Lazaridis, T. Biochimica Et Biophysica Acta-Biomembranes 2007, 1768, 30–38.
22. Li, J.; Das, P.; Zhou, R. J Phys Chem B 2010, 114, 8799–8806.
23. Nobusawa, E.; Aoyama, T.; Kato, H.; Suzuki, Y.; Tateno, Y.; Nakajima, K. Virology 1991, 182, 475–485.
24. Lorieau, J. L.; Louis, J. M.; Bax, A. Proc Natl Acad Sci USA 2010, 107, 11341–11346.
25. Han, X.; Bushweller, J. H.; Cafiso, D. S.; Tamm, L. K. Nat Struct Biol 2001, 8, 715–720.
26. Lorieau, J. L.; Louis, J. M.; Bax, A. J Am Chem Soc 2011, 133, 14184–14187.
27. Han, X.; Tamm, L. K. Proc Natl Acad Sci USA 2000, 97, 13097–13102.
28. Lakomek, N. A.; Ying, J. F.; Bax, A. J Biomol NMR 2012, in press.
29. Mandel, A. M.; Akke, M.; Palmer, A. G. J Mol Biol 1995, 246, 144–163.
30. Yao, L.; Grishaev, A.; Cornilescu, G.; Bax, A. J Am Chem Soc, 2010, 132, 4295–4309.
31. Yao, L.; Voegeli, B.; Ying, J. F.; Bax, A. J Am Chem Soc 2008, 130, 16518–16520.
32. Clarke, S. Int J Pept Protein Res 1987, 30, 808–821.
33. Lorieau, J. L.; Louis, J. M.; Bax, A. J Am Chem Soc 2011, 133, 2824–2827.
34. Lipari, G.; Szabo, A. J Am Chem Soc 1982, 104, 4546–4559.
35. Berjanskii, M.; Wishart, D. S. Nat Protoc 2006, 1, 683–688.
36. Shen, Y.; Delaglio, F.; Cornilescu, G.; Bax, A. J Biomol NMR 2009, 44, 213–223.
37. Blumenthal, R.; Sarkar, D. P.; Durell, S.; Howard, D. E.; Morris, S. J. J Cell Biol 1996, 135, 63–71.
38. Donald, J. E.; Zhang, Y.; Fiorin, G.; Carnevale, V.; Slochower, D. R.; Gai, F.; Klein, M. L.; DeGrado, W. F. Proc Natl Acad Sci USA 2011, 108, 3958–3963.
39. Fleury, D.; Wharton, S. A.; Skehel, J. J.; Knossow, M.; Bizebard, T. Nat Struct Biol 1998, 5, 119–123.

Reviewing Editor: Stephen K. Burley